J. Indian Inst. Sci., 66, Sept.-Oct. 1986, pp. 613-628
© Indian Institute of Science, Printed in India

IISc THESES ABSTRACTS

Thesis Abstract (Ph.D.)

Studies on the realization of varistors with positive voltage coefficient of resistance based on composites by K. Lalkishore.
Research supervisor: M. Satyam.
Department: Electrical Communication Engineering.

1. Introduction

The need for economical voltage regulators is being increasingly felt with the use of electrical and sophisticated electronic appliances, equipment, etc., for various applications. One of the methods by which this can be realized is through functional approach, wherein, the number of components required to perform a given function is minimized. To regulate the voltage, a single device can be connected in series with the load. The resistance of such a device has to increase with the increase in voltage, such that the excess voltage is dropped across the device. Such a device can be termed as a varistor with positive voltage coefficient of resistance (PVCR), since its resistance increases with voltage. Most of the recent research work is confined to zinc oxide varistors which exhibit −ve voltage coefficient of resistance. Barretter, a hydrogen gas filled tube has +ve voltage coefficient of resistance, but it cannot find a place in this age of miniaturization. So there is considerable need to develop varistors with PVCR, which will have very wide practical applications.

The thesis deals with the way in which one realizes PVCR varistors through composites. Three types of materials/structures, *viz.* (1) $BaTiO_3$–graphite–rubber composite samples (2) $BaTiO_3$–graphite–glass frit composite samples (3) PZT–thick film devices have been conceived, prepared and tested. The results of this effort are described below.

(i) *$BaTiO_3$–graphite–rubber samples*

$BaTiO_3$ and graphite powders of specific grain size, taken in a particular proportion, are mixed thoroughly and dispersed in a synthetic rubber solution. The paste is air-dried and pressed into pellets and vulcanized; ohmic contacts are taken using silver paste.

Figure 1 shows the typical variation of resistivity with voltage, derived from the V–I characteristic. The voltage-current relationship is given by the equation,

$$I = KV^n \tag{1}$$

where n is the nonlinearity factor. The voltage coefficient of resistance α_v is defined as

$$\alpha_v = \frac{1}{R}\left(\frac{dR}{dV}\right) \tag{2}$$

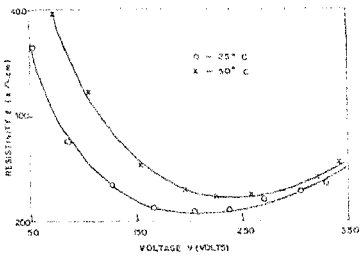

Fig. 1. Variation of resistivity with voltage for sample 1. o: Graphite particles in 'm' layers in the outer cube. O: 'm' $BATIO_3$ particles in a row in the inner cube. (Particles embedded with rubber)

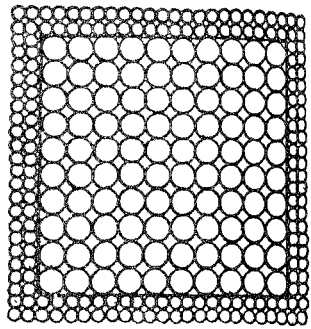

Fig. 2. Cross-section of an elemental cell.

It is found that the resistivity, nonlinearity factor and voltage coefficient of resistance are affected by the composition and particle size. The resistivity is found to decrease initially and then increase beyond a certain voltage.

Explanation

It is known that $BaTiO_3$ particles elongate in the direction of the applied field due to electrostrictive property[1,2]. As they elongate, rubber may also elongate in the same direction due to its elastic nature resulting in the increase in distance between the conducting graphite granules. When a voltage is applied across the specimen, electron emission through tunneling

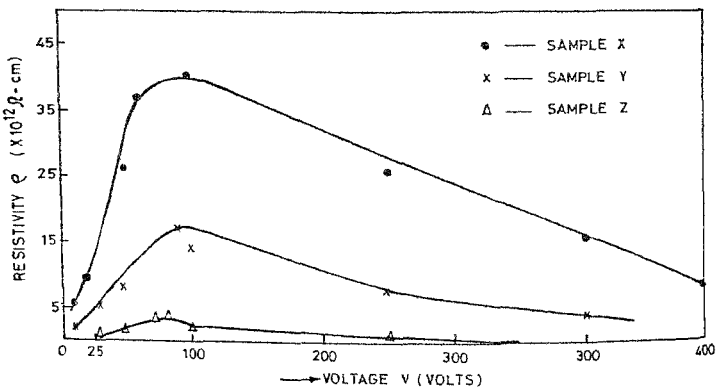

Fig. 3. Variation of resistivity with voltage at room temperature.

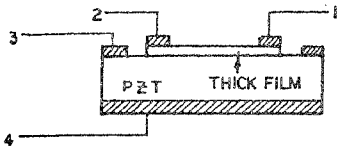

FIG 4. Structure of the PzT-thick film device with four terminals. ▨ silvered portion.

across the gap between the conducting granules takes place and it increases with increase in voltage. However, the increase in the gap-length due to the applied voltage reduces the emission. Hence the $V-\rho$ characteristic is as obtained. A model is proposed on these lines, which assumes that the sample consists of number of elemental cells, the cross-section of which is shown in fig. 2. Theoretical expressions derived based on this model are found to satisfactorily explain the observed results.

(ii) $BaTiO_3$–graphite–frit samples

The rubber samples have the disadvantage of limited temperature range of operation. So rubber is replaced with frit and samples are made. Typical $V-\rho$ characteristics are shown in fig. 3. The resistivity is found to increase with voltage initially and then decrease at higher voltages.

The process that gives rise to the above characteristics seems to be different from that in the previous case. The characteristics in this case seem to be controlled by trapping of charged

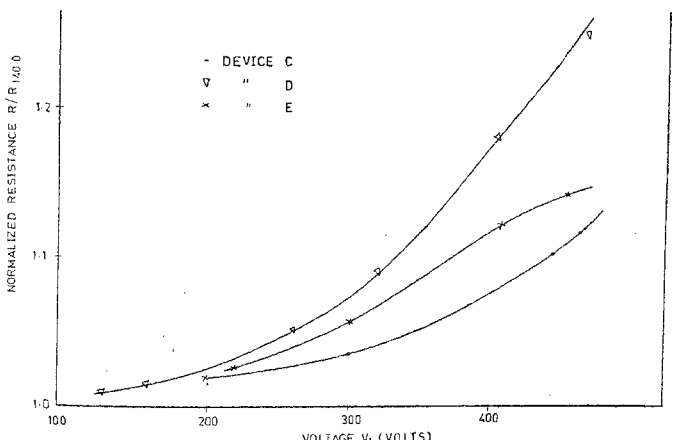

FIG 5. Variation of normalized resistance with voltage V_1 for three devices from experimental results (normalized with the resistance at 140 V).

[illegible] the insulator get trapped and consequently [illegible] voltage takes place. Once the traps are filled, [illegible] the flow of current. This leads to an increase in current and consequently decrease in [illegible].

(iii) *PZT thick film devices*

Another approach has been made in which a thick film of [illegible] is printed on a poled lead zirconate titanate (PZT) disc by screen printing technique. When a voltage is applied to the PZT disc, it undergoes dimensional changes [illegible] and so the resistance of the thick film increases. The structure of the device is shown in Fig. 4. Figure 5 shows typical variation of normalized resistance with voltage.

It is observed that the resistance of the thick film increases with voltage beyond a certain value which is about 140 V. The increase in resistance is more for PZT discs with higher values of d_{33} coefficient. This is due to the fact that piezoelectric effect is considerable at higher voltages and for higher values of d_{33}.

2. Conclusions

This thesis describes three different approaches conceived, samples made, tested and results obtained to realize varistors with positive voltage coefficient of resistance.

References

1. Mason, W. P.	*Piezoelectric crystals and their applications to ultrasonics*, D. Van Nostrand Co.
2. Mason, W. P.	*Phys. Rev.*, 1948, 73(11), 1398.
3. Uchino, K., Cross, L. E. and Newnham, R. E.	*J. Appl. Phys.*, 1981, 52(3), 1455.
4. Burn, I.	*Bull. Am. Ceram. Soc.*, 1971, 50, 501.
5. Turner, R. F.	*Voltage dependent resistors*, Foul Sham-Sams, 1970.
6. Jenkins, R. O.	*Br. J. Appl. Phys.*, 1958, 9(10), 391.

Thesis Abstract (Ph.D.)

Autonomous fault-tolerant spacecraft attitude control system through reconfiguration by S. Murugesan.

Research supervisors: U. R. Rao (ISRO), E. V. Krishnamurthy and N. Viswanadham.
Department: School of Automation.

1. Introduction

Spacecraft play many important roles–domestic and international telecommunication and broadcasting, weather forecasting, remote sensing, military applications, etc. Their services have

become essential in our day-to-day life and there is an ever growing need for uninterrupted operation of spacecraft over a long period (~10–15 years).

Attitude control system (ACS), the heart of a spacecraft, performs the primary task of orientation and maintenance of the spacecraft and/or its payload in a desired direction. ACS consists of various types of attitude sensors and actuators, and control electronics (onboard computer). It becomes more complex when services performed by a spacecraft become sophisticated. Proper functioning of ACS is vital for rendering desired services and for mission success. The major concern is, therefore, to achieve a very high reliability and uninterrupted operation of ACS.

2. Present status and requirements

Despite various efforts to improve reliability of space systems through 'fault-avoidance' techniques such as improvements in design, use of high reliability components, and elaborate and intensive testing, random failures may occur in various subsystems during their long operational life. Although most spacecraft generally have redundant units to avoid 'mission-critical-single-point-failures', they do not have autonomous fault detection and identification and reconfiguration capabilities. Faults are analysed in ground using telemetry information and appropriate actions are taken through telecommand to overcome the effects of failures. This approach, however, invariably leads to a loss of attitude, requiring reacquisition with attendant risks, fuel penalty with consequent reduction in mission life and interruption in service, which is not tolerable in many applications.

To circumvent these, an autonomous fault-tolerant spacecraft attitude control system that continues to function correctly despite failures, without human intervention or ground station support, is required. It essentially calls for fault tolerance in attitude sensors, actuators and control electronics, by the use of functional redundancy.

Various techniques have been developed for fault tolerance in computers. However, as functions, failure modes and redundancy management of sensors and actuators are quite different from that of computer/electronics systems, fault-tolerant computing techniques are not directly applicable to sensors and actuators. For instance, actuators that failed in a continuous actuating mode cannot be left as such by substituting a redundant actuator, as is usually done in computers/electronics systems. The popular triple modular redundancy (TMR) with majority voting is also not applicable to actuators like reaction/momentum wheels.

Constraints for space applications: Also, while dealing with space applications, there are severe constraints on weight, volume, power consumption and locations for mounting of the sensors/actuators. Hence, the number of redundant units have to be kept to a minimum, by adopting some form of dynamic redundancy for attitude sensors and actuators. This necessitates autonomous onboard fault detection, identification and isolation, and reconfiguration of the system. However, algorithms used for these should be as simple as possible without much increase in the hardware and computational complexity. Also, it is desirable that these algorithms are based on existing performance measurements without need for additional monitors/transducers.

But, as yet, suitable autonomous fault tolerance techniques for some of the critical attitude sensors and actuators are not available.

3. Autonomous fault-tolerant system

This work is concerned with the development of autonomous fault tolerance schemes for spacecraft attitude sensors and actuators. Primarily, it deals with methodology and algorithms for fault detection and identification (FDI), and reconfiguration schemes for the sub-systems–such as earth sensors, gyros, reaction momentum wheels and thrusters, reaction control system-RCS)–that are vital and critical for normal on orbit operations and mission success. As the functions, principle of operation and type of failures and their effects are different for each of these subsystems, fault detection and isolation (FDI) schemes for these subsystems differ from each other considerably.

With an emphasis on the need for fault tolerance in attitude control system, an overview of the attitude control system is presented. Also, an outline of the principles and various means of achieving fault tolerance and essential requirements (ten commandments) of a fault-tolerant spacecraft attitude control system are given.

In real life situations 'majority voter', which is commonly used in TMR systems, has a few limitations; alternative schemes such as 'weighted voter' are complex. We, therefore, develop a simple cascadable median selector, using 16 nonvolatile read only-memories (PROMs), for output selection in a TMR system. It is based on a newly developed novel partitioning scheme which decomposes the problem of determination of median of a set of three n-bit data into a sequence of two or more median selection process (steps) with reduced number of bits k ($k < n$). This scheme drastically reduces memory requirement and, hence, the complexity of hardware. For instance, this scheme requires just 8K bytes of memory for 16-bit input data, compared to approximately a half million Giga bytes of memory needed for the direct single-look-up-table approach. This modular hardware median selector is quite useful in a number of applications, including built-in fault tolerance in very large scale integrated (VLSI) circuits.

A description of various types and modes of failures of earth sensor, dynamically tuned gyro (DTG), reaction/momentum wheel and RCS is given and effects of these failures on performance of the control system and on the mission are discussed.

Algorithms are developed for autonomous detection and identification of a faulty earth sensor in a dual-redundant system; they cover stuck up failures, and excessive bias and noise in the output. They are based on outputs of earth sensors, the concept of 'hypothesis testing' and spacecraft attitude behaviour. An autonomous reconfiguration scheme for earth sensors is also given.

For a fault-tolerant attitude reference system using three DTGs, a new symmetrically skewed configuration (fig. 1) is developed. This configuration overcomes the limitations of the other known configurations 2, 3. With a systematic study and analysis, various features such as error in attitude estimate, computational complexity and fault coverage, are compared for different configurations (Table I), and shown that the new configuration is better than the other known configurations.

An algorithm for detection and identification of a faulty reaction/momentum wheel is presented; it covers all the modes of failures of a wheel, that are critical to a mission. The algorithm computes expected change in wheel speed over a period (for the given control signal) and compares it with actual change in wheel speed (over the same period). Also, reconfiguration schemes for 'skewed-four-reaction wheel', dual momentum wheel and hybrid momentum/reaction wheel systems are developed. These involve autonomous modification of controllers'

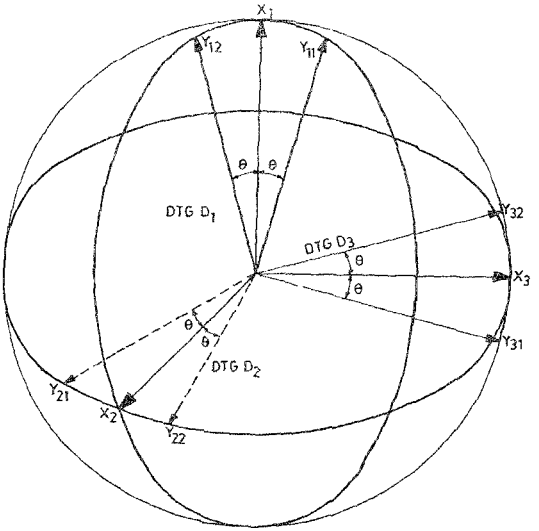

FIG 1 New symmetrically skewed configuration for attitude reference system using three dynamically tuned gyros (DTGs). $\theta = 45°$; DTG D_1 in $X_1 - X_2$ PLANE; DTG D_2 in $X_2 - X_3$ PLANE; and DTG D_3 in $X_3 - X_1$ PLANE

inputs and/or outputs according to the wheel that is faulty. Computer simulations are carried out to validate these algorithms and the results are presented.

Further, for RCS, FDIR schemes that enable continued correct functioning and prevent depletion of propellent, is presented. They cover stuck-at-open, stuck-at-closed and large and small leakage failures.

Also, scope of further work in this new and promising field of 'autonomous spacecraft control' are given.

4. Features

The proposed techniques for fault tolerance in attitude sensors and actuators are suitable for implementation in a spacecraft without much increase in hardware and computational complexity. These techniques are general (or universal) in nature and hence, they could be applied to any spacecraft. Further, they do not call for any modification/redesign of sensors and actuators that are already being used and additional monitors. Also, they, by providing uninterrupted service, enhance utility, life and probability of success of a mission. It may be mentioned that the autonomous reconfiguration scheme for "skewed-four-reaction-wheel" system has already been implemented in the Indian Remote Sensing (IRS) satellite, scheduled for launch.

Table 1
Comparison of various configurations of attitude reference system using three DTGs

Features	Configuration			
	Conventional	Unsymmetrically skewed	Orthogonal	New symmetrically skewed
σ_θ/σ_m *	All DTGs OK	0.707	0.745	0.816	0.707
	One DTG has failed	1.000	1.224	1.414	1.000
Computational requirements	Very little	More	More	Less
Fault tolerance features	Cannot identify a faulty DTG if one of its output is faulty, while the other is correct. Hence it does not provide full fault coverage for a DTG failure	Provides full fault coverage against a DTG failure	Provides full fault coverage against a DTG failure	Provides full fault coverage against a DTG failure
Remarks				Optimum configuration in terms of error in estimated attitude, computational requirements and fault tolerance.

* σ_θ^2: Variance of the error in the attitude estimate; σ_m^2: Variance of the measurement error of DIG.

References

1. BROWN, R. B. — New voter schemes, *J. Dynamic Systems, Measurement Control*, 1975, 41–45.
2. HARRISON, J. V. AND CHEN, T. T. — Failure isolation of a minimally redundant inertial sensor system, *IEEE Trans. Aerospace Electl Systems*, 1975, AES-11, 349–357.
3. ENGELDER, P. D. — DRIMS-A redundant strapdown IMU for booster guidance and control, *Proc. IEEE National Aerospace Conf.*, 1980, pp 330–337.

Thesis Abstract (Ph.D.)

Performance of the eigenvector (EV) method in the presence of coloured noise by Madaka Subbarayudu.
Research supervisor: P. S. Naidu.
Department: Electrical Communication Engineering.

1. Introduction

The subject of determining the number of sources and their bearings from the output of an array of sensors in the presence of noise, is studied in this thesis. Among the various nonlinear spectrum estimation methods the eigenvector method or the Pisarenko method is the latest. The performance of this method in presence of coloured noise is investigated. The method has applications in passive sonar and radar. A suitable model of coloured noise is developed reflecting some aspects of the real life situation.

2. Problem formulation

In practice the source spectral density matrix is computed from the output of the array from which we get only an estimate of the true spectral density matrix. In this study, it is assumed that the source spectral density matrix is exactly known. For the selection of suitable noise field, a physical model of noise sources concentrated over a finite arc of a circle of infinite radius has been investigated and a complete analysis of the spectral characteristics of the noise model, called the sector background noise, is provided. This is a generalization of earlier results, derived for a model where the noise sources are concentrated over an infinite circle and sphere[1]. Now the model consists of a known source spectral density matrix in the presence of the sector background noise matrix. Then the performance of the EV method is studied on the above model. Further, the performance of the method in presence of estimation errors *i.e.* when only an estimate of the spectral density matrix is available, is investigated. The eigenvector method is applied for detection and estimation of an extended source, an idea based on a special pattern of peaks observed when the background noise is due to a sector noise model.

The method basically consists of decomposing the spectral density matrix (source spectral density matrix plus the spectral density matrix of the background noise) into its eigenvalues and eigenvectors. The set of eigenvalues is called the eigenstructure. The eigenstructure consists of a group of equal and small eigenvalues, hereafter called noise eigenvalues. The rest are large and called signal eigenvalues. The eigenstructure is used to determine the number of signal sources.

In this method the noise eigenvalues and the orthogonal property of the noise eigenvectors are exploited to determine the number of sources and their bearings[1]. A technique known as prewhitening[2] is used to spatially whiten the sector background noise.

3. Results and discussion

The main contributions are:

(1) When the signal is associated with sector background noise, the detection of single source c two sources is not possible by observing the eigenstructure. However, prewhitening can be use to advantage to detect a single source.

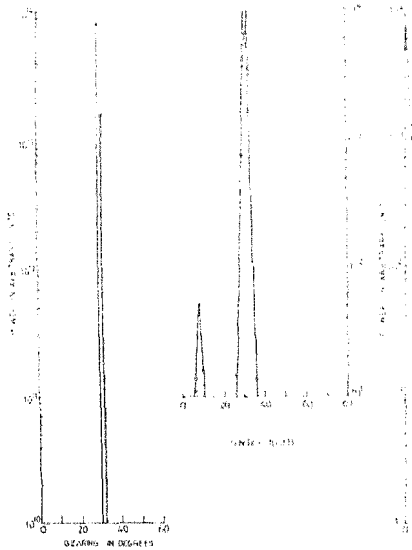

FIG. 1. PSD vs bearing, two sources, sector noise, no prewhitening.

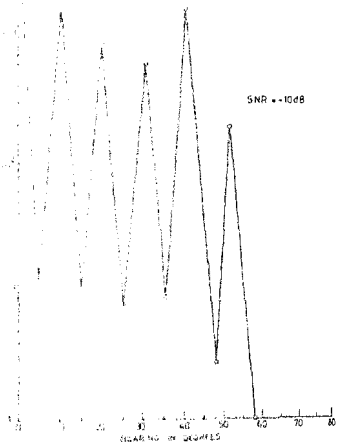

FIG. 2. PSD vs bearing, two sources, sector noise, prewhitened.

(2) Resolution of two sources separated by 2° in the presence of sector noise requires an SNR of 30 dB if the smallest noise vector is used or an SNR of 20 dB, if the average of all the noise eigenvectors is used. Thus averaging provides improvement in resolving two sources. The effect of averaging is shown in figs. 1 and 2.

(3) Without prewhitening, a minimum of 20 dB is required to detect a single source, whereas after prewhitening the same could be detected even at as low as SNR of −10 dB.

(4) In order to prewhiten the coloured noise, the noise sector width should be known within ±10%. Thus prewhitening method is relatively robust.

(5) The detection probability as a function of estimation errors caused by finite data length increases exponentially with decreasing variance.

(6) For an extended source with angular width greater than ±0·125°, from the eigen-spectrum it is observed that there are more than one signal peak along with comparable side lobes. Such a special structure of the eigen-spectrum can be used for detection and estimation of an extended source. The width can be estimated with an accuracy of ±0·208%.

4. Conclusion

The thesis examined the role of sector-background noise and the effect of estimation errors on the bearing estimation of a point source. It further looked into the application of the method to the detection and estimation of an extended source.

References

1. Jacobsen, M. J. Space-time correlation in spherical and circular noise fields, *JASA*, 1962, **34** (7), 971–978.

2. Bienvenu, G. Influence of the spatial coherence of the background noise on high resolution passive methods, *Proc. ICASSP 79*, Washington DC, 2–4 April 1979, 306–309.

Thesis Abstract (M.Sc. Engng)

Studies on sound transmission in shallow sea by C. Karthikeyan.

Research supervisor: G. V. Anand.
Department: Electrical Communication Engineering.

1. Introduction

Modelling of acoustic propagation in the sea has become a subject of great current interest. Besides being of immediate relevance to sonar and underwater communication systems, propagation of acoustic signals in the sea is now being utilized as a method for investigation and monitoring of many fundamental oceanic processes. In all applications, the acoustic transmission loss is an important parameter. In general, transmission loss depends on the prevailing oceanographic and meteorological conditions, the geology and topography of the sea bottom, and the frequency and depth of operation of the sonar transmitter and receiver. This complex dependence of transmission loss on a large number of parameters makes the development of a general transmission loss model quite difficult. This is especially so in shallow sea where the sound field involves the interference of multiply reflected sound waves at the rough boundaries. The problem can get further complicated when there is a sloping sea bottom or when the water and sediment layers are not perfectly stratified. Both the wave-theoretic (normal mode) and the ray-theoretic approaches have been used for modelling sound propagation in shallow sea, although the normal-mode approach is often preferred, especially at lower frequencies or in shallow water.

The present work is devoted to the study of two problems: (1) development of an improved model of attenuation of normal modes, and (2) development of a model of sound transmission in a shallow horizontally stratified ocean using the ray theory.

2. Frequency dependent attenuation of normal modes

In its simplest form, the normal mode theory is based on the Pekeris model of the ocean[1]. This model considers the sea to consist of a layer of homogeneous lossless fluid of constant thickness overlying a homogeneous lossless fluid half-space of higher density and sound speed. The theory

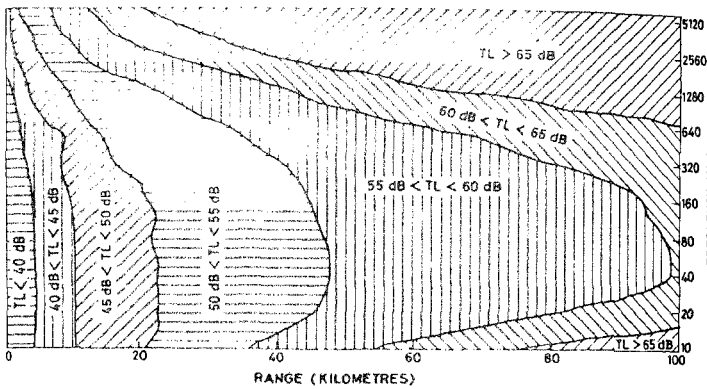

FIG. 1. Range-frequency plot of transmission loss in a 200 m deep Pekeris channel with $C_1 = 1540$ m/sec and $C_2 = 2030$ m/sec

of Pekeris was extended by Kornhauser and Raney[2] to include the effect of a sound-absorbing sea bottom. In the present investigation the normal mode theory is extended to include the effect of sound absorption in sea water. The frequency dependance of sound absorption in the sea bottom sediments and in sea water are discussed and it is shown that the resulting expression for the attenuation of normal modes gives a band-pass characteristic to the channel for each propagating mode. Next, the effect of scattering at the rough sea surface, as determined by Kuperman and Ingenito[3], is included in the model for the computation of modal attenuation. A computer program is developed for the computation of sound transmission loss by coherent addition of normal modes. The results are presented in fig. 1 as a contour plot in the range-frequency plane. The plot clearly shows the existence of an optimum frequency band for sound transmission in shallow sea.

3. Ray theoretic sound transmission model for shallow sea

Extension of the normal mode theory to more realistic models of the ocean is fraught with many mathematical difficulties. The ray theory represents an attempt at circumventing these difficulties. But, while the ray theory provides a good approximation to the boundary value problem of sound transmission in deep sea, it leads to incorrect results in shallow water especially at low frequencies. Recently, Tindle and Bold[4] developed an improved ray theory and obtained results for the Pekeris channel which are in good agreement with the normal mode results. According to the improved ray theory, whenever a ray undergoes total internal reflection at the interface between two homogeneous media, it undergoes a lateral displacement Δ parallel to the interface given by

$$\Delta = -\frac{\partial \phi}{\partial k}$$

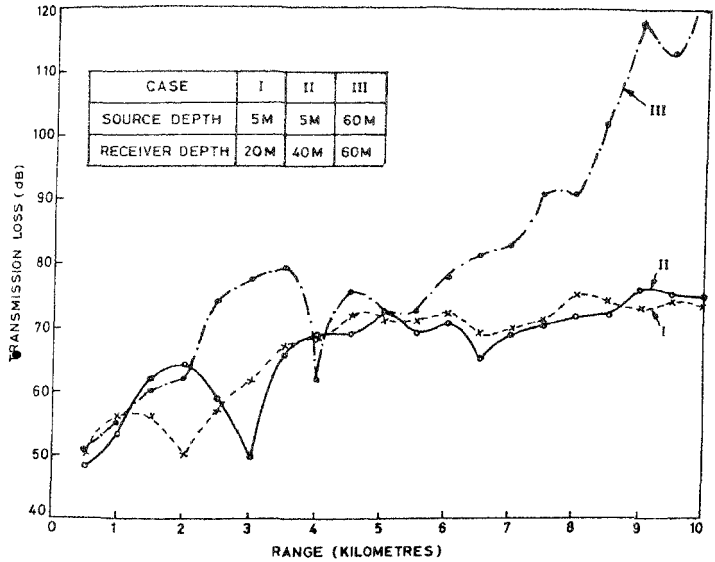

FIG. 2 Transmission loss at 200 Hz, in a 65 m deep channel for three combinations of source and receiver depths.

where ϕ is the phase of the plane wave reflection coefficient and k is the component of wave number parallel to the interface. In the present study, the improved ray theory is applied to develop a sound transmission model for shallow sea with a bilinear sound speed profile consisting of a surface layer with a positive sound speed gradient overlying a layer with a negative gradient. For a given configuration of the source and the receiver, all the eigenrays, *i.e.*, rays joining the source and the receiver are identified and the amplitude and phase of each eigenray at the receiver are computed. Attenuation due to absorption in water, absorption in the sea bottom, and scattering at the sea surface are taken into account in these computations. The acoustic field at the receiver is obtained by coherent addition of the fields contributed by all the eigenrays. However, if the surface of the ocean is rough and the phases of the eigenrays can be considered to be uncorrelated, an incoherent summation (addition of intensities) is carried out. An algorithm based on this technique is developed for computation of the transmission loss and also for the prediction of the waveform of the received signal. Computed results for the variation of transmission loss with range for a typical ocean channel are shown in fig. 2. These results and others based on similar computations are found to agree well with results obtained from the normal mode theory.

References

1. Pierce, C. T. — Theory of propagation of explosive sound in the ocean, *Geol. Soc. Am. Mem.*, 1948, **27**, 1–117.

2. Kibblewhite, E. J. and Ewans, W. P. — Attenuation in shallow water propagation due to an absorbing bottom, *J. Acoust. Soc. Am.*, 1985, **27**, 689–692.

3. Kuperman, W. A. and Ingenito, F. — Attenuation of the coherent component of sound propagating in shallow water with rough boundaries, *J. Acoust. Soc. Am.*, 1977, **61**, 1178–1187.

4. Thorp, C. T. and Bold, G. E. J. — Improved ray calculations in shallow water, *J. Acoust. Soc. Am.*, 1981, **70**, 813–819.

Thesis Abstract (M.Sc. Engng)

Analytical study of some aspects of crosstalk in wavelength division multiplexing-based fiber-optic systems by S. Narasimha Prasad.
Research supervisor: S. V. Pappu.
Department: Electrical Communication Engineering.

1. Introduction

Wavelength Division Multiplexing (WDM) technique has been a source of significant potentiality in the fiber optic communication systems[1–4]. It allows the augmentation of the information carrying capacity of a given channel. In this technique a number of individually modulated distinct optical wavelengths, known as optical signals, are combined and allowed to propagate along a single fiber. At the receiving end, each optical signal is extracted from the composite signal by spectral dispersion and then is subjected to the processes of detection and demodulation. The combining and dispersing actions are achieved through a multiplexer and demultiplexer respectively. In the light of evolving fiber-optic technology the designer encounters several obstacles in extracting out the optimal utilization performance of the potentialities offered by this WDM technique and these should either be eliminated or kept at minimum. The crosstalk which refers to the unwanted coupling of optical signals is one such parameter of considerable significance.

Crosstalk arises due to various causes and several among them have been studied[5–8]. This thesis describes an analytical study made on that which arises out of overlapping of emission spectra of optical sources used. This cause becomes predominant when one attempts to enhance the channel count in a restricted transmission band of an optical fiber. We refer to this crosstalk as Interchannel Crosstalk (ICC) and the study made is intended to arrive at an *a priori* estimation of it in order to select necessary types of sources.

2. Analysis of ICC

The most general definition for ICC, C in dB is

$$C(dB) = 10 \log \left(\frac{\text{Disturbing optical power}}{\text{Disturbed optical power}} \right).$$

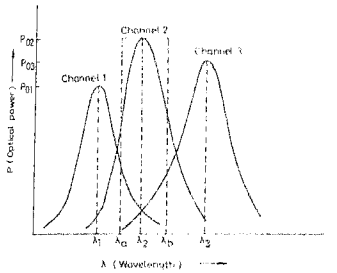

Fig. 1. Schematic diagram to illustrate ICC arising due to overlapping emission spectra of adjacent channels. λ_1, λ_2 and λ_3 are peak wavelengths with peak optical powers P_{01}, P_{02} and P_{03} in channels 1, 2 and 3 respectively. ($\lambda_b - \lambda_a$) indicates the width of filter window.

A schematic diagram depicting the situation of overlapping of spectral profiles of three sources (or channels) is shown in fig. 1.

The actual crosstalk will differ from the ideal value ($-\infty dB$) depending on the amount of overlap. ICC values can be calculated in a given situation either, (i) by considering powers (or intensities) with reference to the peak wavelengths of the sources, or (ii) within a finite demultiplexer (filter) window of a desired channel. Based on these two cases, ICC analysis has been carried out in two ways, namely, theoretically and graphically. In regard to the theoretical analysis we have deduced the equations to estimate crosstalk by the following methods:

(a) by fitting Gaussian equation to the emission spectra of sources,

(b) graphical method of computing ICC using the realistic source profiles provided by the manufacturer,

(c) by fitting Gaussian distribution relation to the emission spectra of sources, and

(d) by fitting Lorentzian distribution relation to the emission spectra of sources.

3. Results and conclusions

By considering the above methods, we have derived appropriate relations for ICC under various situations. Using these equations, model calculations done are presented. The graphical method that we have discussed is applicable when realistic source emission spectra are given by the manufacturers of optical sources. ICC values are computed for two sets of typical sources whose relative intensity wavelength graphs are given using this method. A comparative study is also made among the methods mentioned.

From our analysis it is found that untolerable limits of crosstalk between adjacent channels can arise at the transmission end itself especially in a high channel count WDM system due to the

overlap of emission spectra of optical sources used. Sources with Gaussian spectral distribution functions are preferable to those sources with limit of Lorentzian or those with gradually falling edges. The graphical method of computation of ICC gives more accurate results than other methods discussed. Using analytical results obtained one can carry out an *a priori* computation of ICC for the design of a WDM system. The method of ICC computation at peak wavelengths is sufficient to arrive at an approximate estimation for system design purposes. Also it is shown that narrower the width of filter window higher is ICC.

References

1. Tomlinson, W. J. — Wavelength multiplexing in multimode optical fibers, *Appl. Opt.*, 1977, 16(6), 2180–2194.
2. Terada, Mio and Hideki Ishio — Variables of the wavelength division multiplexing transmission system over an optical fiber cable, *IEEE Trans. Commun.*, 1978, Com-26(7), 1082–1087.
3. Hideki Ishio *et al* — Review and status of wavelength division multiplexing technology and its application, *J. Lightwave Technol.*, 1984, LT-2(4), 448–463.
4. Gerhard Winzer — Wavelength multiplexing components – A review of single mode devices and their applications, *J. Lightwave Technol.*, 1984, LT-2(4), 369–378.
5. Wells, W. H. — Crosstalk in a bidirectional optical fiber link, *Integr. Opt.*, 1978, 1, 243–287.
6. Aoyama *et al* — Crosstalk due to spontaneous Raman scattering in WDM transmission systems, *Proc. IOOC-83*, 1983, 27C2–3.
7. Tomita, A. — Crosstalk caused by stimulated Raman scattering in single mode wavelength division multiplexed systems, *Opt. Lett.*, 1983, 8(7), 412–414.
8. Hill, A. M. and Payne, D. B. — Linear crosstalk in wavelength division multiplexed optical fiber transmission systems, *J. Lightwave Technol.*, 1995, LT-3(3), 643–650.